3D numerical simulations of a transitional axisymmetric synthetic jet

C. Fischer and R. Sharma

Department of Mechanical Engineering
University of Auckland, Auckland 1142, New Zealand

Abstract

Synthetic jets have been an area of interest in the recent years with constantly increasing industrial demand. Application areas are widespread and a strong focus is put on boundary layer control and mixing enhancement. A synthetic jet at a jet Reynolds number of Re_d=18 000 has been studied using physical experiments involving hot wire anemometry and three-dimensional transient numerical simulations. The k-ε model, the k-ω based SST model, and the hybrid turbulence model SAS are used for the numerical simulations where mean flow data and second order turbulence statistics are compared to data from the physical experiments. In the synthetic jet flow field vortex interaction is present. Therefore, the capability of the different turbulence models to resolve the transitional three-dimensional jet flow is discussed and assessed.

Introduction

Flow controlling gadgets such as synthetic jet actuator (SJA) have been an area of interest for more than 20 years with constantly increasing industrial demand. Application areas for synthetic jets (SJ) include flow separation control, cooling, thrust vectoring, and sound emission reduction. Hence, a strong focus is put on boundary layer control [5, 7, 17] and mixing enhancement [6, 12, 18].

An SJA setup typically consists of a cavity containing an oscillating membrane, which is often opposite the orifice. The shape and volume of both, cavity and orifice, can vary from round through square to rectangular shapes. Commonly used actuators are piezo-electric disks, pistons, and loudspeakers. Axisymmetric or three-dimensional (3D) jets are synthesised from round orifices. Jets generated from rectangular orifices are termed planar or two-dimensional (2D) jets. In contrast to the continuous jet, the SJ does not need an additional fluid supply. This feature makes the SJ attractive for numerous applications. Furthermore, the SJ is developed from ambient air, and thus, the net mass flux over a cycle is zero. A SJ is therefore also referred to as a zero-net-mass-flux jet.

During a cycle, the membrane undergoes a sinusoidal motion, alternately pushing ambient air out of and sucking air into the cavity. The expulsion part of the cycle is characterised by vortical structures that can roll-up and move away from the orifice. The shape and size of these structures strongly depend on the orifice geometry and on the actuator settings. These include actuator amplitude and frequency. Vortex roll-up is only ensured if certain criteria are fulfilled. Initial conditions such as actuator frequency, amplitude, cavity volume, orifice shape, etc. vary largely in the different studies presented in the literature. Hence, there is still limited systematic information on vortex formation, vortex interaction, and phenomena such as axis-switching.

Computers have become a suitable tool to investigate SJ flows. Computational Fluid Dynamics (CFD) have been utilised for SJ flow studies to get detailed flow field information, as they are often limited in physical experiments. In the published literature, the following types of numerical simulations can be found:

- 2D simulations using two-equation turbulence models [2, 4] or Direct Numerical Simulations (DNS) [8] or

- 3D laminar simulations [18] or 3D Large Eddy Simulations (LES) [5, 16].

In this study two different two-equation turbulence models, namely the k-ε and the SST model, and the hybrid Unsteady Reynolds Averaged Navier–Stokes (URANS) turbulence model – Scale Adaptive Simulation-Shear Stress Transport (SAS-SST) – were used for the numerical simulations. The models were assessed due to their ability to resolve the complex jet flow. Additionally, the numerical data was validated against hot wire anemometer (HWA) data. The validation included the comparison and analysis of centreline velocity decays and volume flows.

Numerical Simulations

The commonly used two-equation turbulence models, such as the k-ω and k-ε models, compute the turbulence length scale L. Kolmogorov, who developed the first two-equation turbulence model, postulated that:

$$l \sim \sqrt{k}/\omega \qquad (1)$$

by developing Prandtl's mixing model further. k is the turbulence kinetic energy and ω is the turbulence eddy dissipation frequency. His research is basis for the standard k-ω model.

k-ω and k-ε

The turbulence length scale, L, in the k-ω model is:

$$L = k^{1/2}/\omega \qquad (2)$$

Whereas in the k-ε model, the turbulence length scale is calculated as follows:

$$L = c_\mu\, k^{3/2}/\varepsilon \qquad (3)$$

where c_μ=0.09 and ε is the eddy dissipation rate. The two models have their advantages and disadvantages, which are shown in Table 1.

Model	Advantage	Disadvantage
k-ω	Boundary layer is resolved	Free stream sensitivity
k-ε	Free stream turbulence resolved	Viscous sublayer not resolved; reduced/suppressed stall

Table 1. Comparison of k-ε and k-ω model.

In order to make use of the advantages of each of the k-ω and k-ε model, a combination of both was developed.

SST

The shear-stress transport model (SST) by Menter utilises a formulation where the k-ω model is used in the near wall region and the k-ε model in the free stream region. This is realised using a blending function in the ω-equation [1]:

$$\frac{\partial(\rho\omega)}{\partial t} + \frac{\partial}{\partial x_j}(\rho\bar{u}_j\omega) = +\frac{\partial}{\partial x_j}\left[\left(\mu+\frac{\mu_t}{\sigma_{\omega2}}\right)\frac{\partial\omega}{\partial x_j}\right]$$
$$+(1-F_1)2\rho\frac{1}{\sigma_{\omega2}\omega}\frac{\partial k}{\partial x_j}\frac{\partial\omega}{\partial x_j} \qquad (4)$$
$$+\alpha_2\frac{\omega}{k}P_k-\beta_2\rho\omega^2$$

Further details on the model constants and the blending function F_1 can be found in [1]. F_1 is a *tanh*-function and is based on the distance to the nearest wall. Thus, F_1 gets 0 or 1 and switches between k-ε in the free stream region and k-ω in the near wall region respectively. The SST model also utilises a limiter for the eddy viscosity because the model cannot account for the transport of the turbulent shear stresses and therefore over-predicts the turbulence eddy viscosity [1]:

$$\mu_t=\rho\frac{\alpha_1 k}{max(\alpha_1\omega,SF_2)} \qquad (5)$$

where $\alpha_1=5/9$ and F_2 is another *tanh*-function. This limiter function allows for modelling of wall bonded shear flows, hence the name shear-stress transport.

The commonly used two-equation turbulence models can resolve good overall predictions for mean flow statistics. However, they fail in computing second order statistics, as they are unable to break up unsteady flows into a turbulent spectrum. DNS and LES do have this ability but also have explicit grid requirements and rely on proper time step selection. This, however, involves high computational costs and resources. An alternative to the these CFD methods is using a hybrid turbulence model such as Detached Eddy Simulation (DES) or Scale Adaptive Simulation (SAS) as they result in higher order simulation data at moderate computational costs.

SAS-SST

Due to its advantages in the near wall region, the SST model is used as basis for the SAS formulation (Q_{SAS}) which is incorporated in the ω-equation. Thus, the ω-equation reads [1]:

$$\frac{\partial(\rho\omega)}{\partial t}+U_j\frac{\partial(\rho\omega)}{\partial x_j}=\alpha\frac{\omega}{k}P_k-\rho\beta\omega^2$$
$$+\frac{\partial}{\partial x_j}\left(\left(\mu+\frac{\mu_t}{\sigma_\omega}\right)\frac{\partial\omega}{\partial x_j}\right) \qquad (6)$$
$$+(1-F_1)\frac{2\rho}{\sigma_{\omega2}}\frac{1}{\omega}\frac{\partial k}{\partial x_j}\frac{\partial\omega}{\partial x_j}+Q_{SAS}$$

where $\sigma_{\omega2}=\sigma_\omega$ in the k-ε regime and $P_k=\mu_t S^2$. Q_{SAS} reads:

$$Q_{SAS}=\rho\cdot max\left[\zeta_2\kappa S^2\left(\frac{L}{L_{vK}}\right)^2-C\frac{2}{\sigma_\Phi}k\right.$$
$$\left.\cdot max\left(\frac{1}{\omega^2}\frac{\partial\omega}{\partial x_j}\frac{\partial\omega}{\partial x_j},\frac{1}{k^2}\frac{\partial k}{\partial x_j}\frac{\partial k}{\partial x_j}\right),0\right] \qquad (7)$$

where $\zeta_2=3.51$, $\sigma_\Phi=2/3$, and $C=2$. Q_{SAS} is zero in the boundary layer and utilises L_{vK} in transient regions.

$$L_{vK}=\kappa\left|\frac{\partial U/\partial y}{\partial^2 U/\partial y^2}\right| \qquad (8)$$

κ is the von Kármán constant and U is the velocity in x direction. L_{vK} allows for small-scale resolution in unsteady regions so that the turbulent structures are resolved due to the mesh size used in the simulation, a more accurate prediction of μ_t, and the development of a turbulent spectrum. $L=\kappa y$ and $L\sim\delta$. Thus, the calculated turbulence length scale is proportional to the boundary layer thickness in the boundary layer region and in dimensions of L_{vK} in unsteady regions. The turbulence model was therefore named Scale Adaptive Simulation. For further theory, for example on damping and limitation of L, derivation of other two-equation and one-equation models, derivation of a viscous sublayer model (VSM) etc., on the SAS model the reader is referred to [9-11].

Experimental Setup

The actuator used in this research was a loudspeaker, being an 8" woofer with a frequency response of 38Hz–4.5KHz. The operating frequency of the woofer was f_d=40Hz (f_d=1/T_d). The woofer amplitude was kept at A_d=1.25mm by constantly measuring the diaphragm displacement with a laser vibrometer. A function generator and an amplifier were used to keep the signal at a constant operating frequency and amplitude. The SJA cavity had a round orifice with a diameter of d_o=20mm and an orifice plate thickness of l_o=9mm. The cavity height was h_c=100mm and the cavity volume was 27×10^5mm^3. Velocity measurements in the jet flow field were taken using a single HWA. The HWA was calibrated before the measurements and a third order correction function was used for the data analysis. The sampling frequency of the HWA was 8KHz and the sampling time was 1.25s. The SJA setup resulted in S=81, L=8.6 and Re_d=18 000 for the presented data based on definitions of [13]. Therefore, the SJ is in the transitional jet region [3].

Numerical Setup

In the numerical model, (ANSYS CFX 13) the loudspeaker movement was realised by applying a moving mesh. Therefore, the diaphragm was moving in a sinusoidal motion using an expression function. The movement of the "rubber" ring around the diaphragm was unspecified thereby allowing for the moving mesh. All other parts in the computational domain were kept stationary. The domain above the orifice was a cube with $20d_o$ edge length. The outlets around and above the orifice were defined as openings (0Pa relative pressure) with low turbulence intensity (1%) at the sides and high turbulence intensity (10%) at the top. The orifice plate and all remaining parts were no slip walls. The fluid was "Air Ideal Gas" at 21°C. The time step size of t_{step}=T_d/2000 resulted in a maximum Courant number smaller than 1. The convergence criteria were set to RMS=1×10^{-5}. The High Resolution advection scheme and a second order backward Euler transient scheme were used.
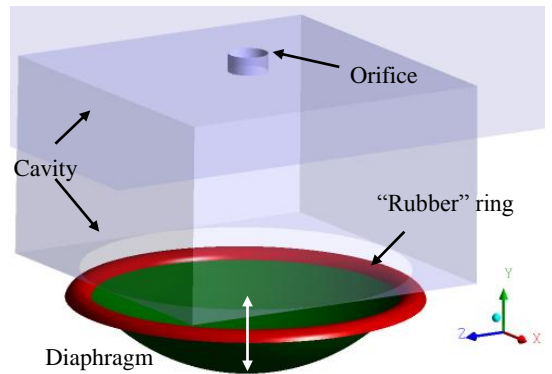

Figure 1. Schematic of the numerical model.

The solver was run in double precision and all remaining settings were kept as default. The mesh used in these simulations was a block structured hexahedral mesh that was built in ICEM CFD and consisted of 3.8×10^6 nodes.

Results

The first comparison made was quantitative and therefore the computational times for a singular cycle have been compared. With increasing complexity of the turbulence model, it is expected that the computational effort will increase. It was not surprising that the k-ε model needed least time and the SAS model the most. However, it was surprising that the difference in computational time was small as it can be seen in Table 2.

Model:	k-ε	SST	SAS
Average CPU time:	1d 8h 28min	1d 9h 14min	1d 9h 26min

Table 2. Computation time for one cycle.

2.3% of the total time of the model k-ε was need additionally for the SST model. Even less, about 1% of the total time of the SST model was need for the SAS model. Therefore, the advantage in using a less complex turbulence model in terms of computational costs was marginal. The following comparisons were qualitative and also show data comparisons resulting from first and second order statistics.

One of the flaws of two-equation turbulence models is the over prediction of the turbulence eddy viscosity. The eddy viscosity ratio is given by:

$$EVR = \mu_t/\mu \qquad (9)$$

EVR and L are shown in Table 3 for the three different turbulence models. The difference between the k-ε and the SST model was small for both, EVR and L. However, EVR was 3.5 times higher compared to the prediction of the SAS model. High $EVRs$ resulted from an over prediction of μ_t. L was almost twice the size when comparing the results from the k-ε and the SST model to that of the SAS model. For the former cases, the size of L related to δ but for the latter case L related to L_{vK}. Thus, the resolution of small scales computed by the SAS model was not limited to the boundary layer thickness but by the mesh size in the computational domain.

Model:	k-ε	SST	SAS
EVR:	544	569	156
L:	9.9mm	9.4mm	5.2mm

Table 3. Comparison of eddy viscosity ratio and turbulence length scale.

Figure 2 shows the average orifice exit velocity, V_o, normalised by the maximum orifice exit velocity for one cycle. At the beginning of the cycle, the fluid was sucked into the cavity, causing a negative velocity. In the middle of the cycle the velocity profiles showed a peak which was caused by the primary vortex ring being shed. The second peak was caused by additional vortex roll-up barely noticeable for the results of the k-ε model. The SST and the SAS model were able to reproduce the flow at the orifice exit, which is dominated by boundary layer flows in the neck of the orifice. However, further downstream of the orifice the flow is expected to be dominated by freestream turbulence, large vortices and small-scale vortex interaction.
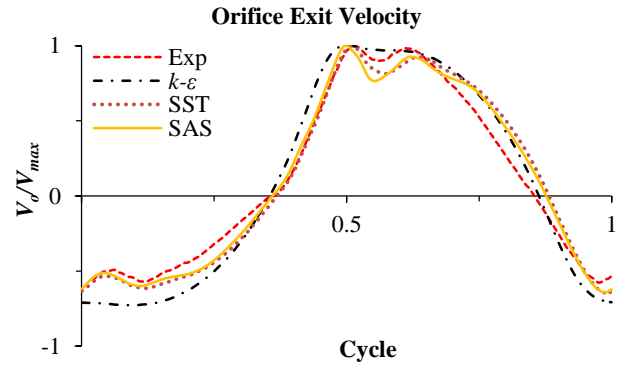

Figure 2. Normalised orifice exit velocity.

The centreline jet velocity, V_{cl}, is decreasing with increasing distance away from the orifice exit. Figure 3 shows the centreline velocity decay where the centreline velocity is normalised with the average orifice exit velocity. For y/d_o=1.5 the SST and the SAS model give good predictions whereas the k-ε over predicts the velocity decay. For y/d_o>2 the velocity decay is well predicted by the k-ε and the SAS model. The SST model underpredicts the velocity decay in this region. For y/d_o>8 vortex interaction causes the jet velocity deceleration. In this region, the k-ε model predicts a linear continual velocity decay whereas the SAS model is able to resolve the flow more correctly. The SST model fails in computing the correct velocity decay. However, the predicted slopes for the decay in the different regions are similar to those of the SAS model.
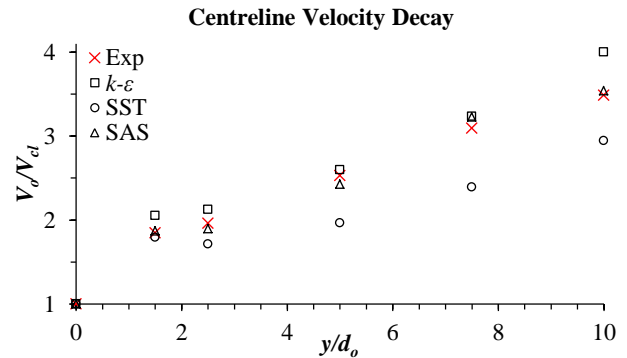

Figure 3. Normalised centreline velocity decays from physical and numerical experiments.

Apart from the jet centreline velocity, the jet flow field can be described by the volume flow. The jet velocity was decreasing downstream as the jet was in size. The jet widened mainly due to the primary vortex ring that was growing constantly while moving away from the orifice exit. The volume flow was calculated via:

$$Q_o = (\pi/4)d_o^2 V_o \qquad (10)$$

Q was calculated using the jet half-with b_j and V_{cl}. The jet half-width was taken as the radial distance from the centreline to the point where the jet velocity was half the average centreline velocity.

Figure 4 shows the volume flow in the measured flow field up to y/d_o=10. Close to the orifice for y/d_o<2 all three models closely matched the experimental data. For y/d_o=2.5 only the SST model predicted a lower volume flow. Further away from the orifice the k-ε model predicted a linear increase which was always lower than the experimental data. The SST model predicted a hyperbolic increase that was similar to that of the experiments

but the predictions in general were too low. The SAS model gave a close fit to the experimental data. However, the data was always slightly lower.

The predictions for the volume flow from each turbulence model followed the trend given for the centreline velocity decays. Finally, the predictions from the SAS matched the experimental data the closest.
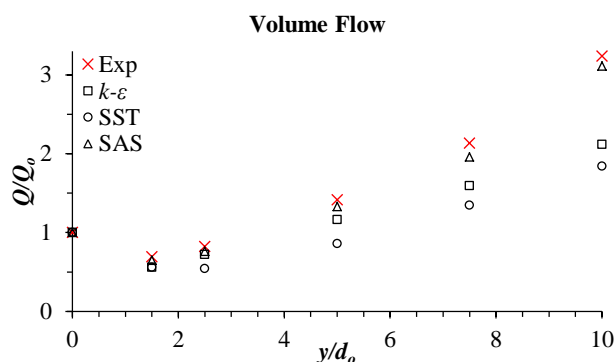
Volume Flow

Figure 4. Normalised volume flow data from physical and numerical experiments.

Conclusions

A synthetic jet at a Reynolds number of Re_d=18 000 was studied in this paper. The comparison of experimental and numerical data showed agreement close to the origin of the jet, but further downstream where vortex dynamics dominate the jet flow the k-ε and the SST model showed deviation from the experimental data. The data from each turbulence model showed consistency throughout the analysed data. It also showed the different limits and abilities of each model due to their varying characteristics. The k-ε and the SST model gave good predictions in areas of the flow field where different dynamics were present. However, they both failed to give an overall reliable prediction. The SAS model was able to resolve the transitional flow field to some degree. It is therefore the most potential turbulence model of the three used models to study SJ flows.

References

[1] ANSYS CFD-Solver Theory Guide: Release 12.0, April 2009.

[2] Carpy, S. and Manceau, R., Turbulence Modelling of Statistically Periodic Flows: The Case of the Synthetic Jet, *Engineering Turbulence Modelling and Experiments*, **6**, 2005, 127–136.

[3] Cater, J.E. and Soria, J., The evolution of round zero-net-mass-flux jets, *J. Fluid Mechanics*, 2002, Vol. **472**, 2002, 167–200.

[4] Chila, R.J. and Kaminski, D.A., Numerical analysis of a synthetic jet using an automated adaptive method, *Int. J. Numer. Meth. Fluids*, 2011, doi: 10.1002/fld.2551.

[5] Dandois, J. and Garnier, E., Unsteady simulation of a synthetic jet in a cross-flow, *AIAA Journal*, **44**, No. 2, 2006, 225–238.

[6] Gillespie, M.B., Black ,W.Z., Rinehart, C. and Glezer, A., Local convective heat transfer from a constant heat flux flat plate cooled by synthetic air jets, *J. Heat Transfer*, **128**, Iss. 10, 2006, 990–1000.

[7] Gordon, M., Cater, J.E. and Soria, J., Investigation of the mean passive scalar field in zero-net-mass-flux jets in cross-flow using planar-laser-induced fluorescence, *Physics of Fluids*, **16**, No. 3, 2004, 794–808.

[8] Lee, C.Y. and Goldstein, D.B., Two-Dimensional Synthetic Jet Simulation, *AIAA Journal*, **40**, No. 3, 2002, 510–516.

[9] Menter, F.R. and Egorov, Y., Formulation of the Scale-Adaptive Simulation (SAS) model during the DESider Project, In: Haase W., Braza M., Revell A. (eds.) *Notes on Num. Fluid Mech. and Multidisc, Design*, Vol. **103**, 2009, 51-62.

[10] Menter, F.R. and Egorov, Y., SAS Turbulence Modelling of Technical Flows, In: *Proceedings of Direct and Large Eddy Simulation*, Netherlands: Springer, 2005, 687-694.

[11] Menter, F.R., Egorov, Y. and Rusch, D., Steady and Unsteady Flow Modelling Using the k-√kL Model. *Turbulence, Heat and Mass Transfer 5*, Begell House, 2006.

[12] Pavlova, A. and Amitay, M., Electronic cooling using synthetic jet impingement, *J. Heat Transfer*, **128**, 2006, 897–907.

[13] Smith, D.R. and Glezer, A., The formation and evolution of synthetic jets, *Physics of Fluid*, Vol. **10**, No. 9, 1998, 2281-2297.

[14] Trávníček, Z. and Tesař, V., Annular synthetic jet used for impinging flow mass-transfer, *Int. J. Heat Mass Transfer*, **46**, 2003, 3291–3297.

[15] Wilcox, D.C., Turbulence modeling for CFD, DCW Industries, Inc., La Canada, 1994.

[16] Wu, D.K.L. and Leschziner, M.A., Large-Eddy Simulations of circular synthetic jets in quiescent surroundings and in turbulent cross-flow, *Int. J. Heat Fluid Flow*, **40**, 2009, 421-434.

[17] Zhong, S., Millet, F. and Wood, N.J., The behaviour of circular synthetic jets in a laminar boundary layer, *Aeronautical J.*, **109**, No. 1100, 2005, 461–470.

[18] Zhou, J., Tang, H. and Zhong, S., Vortex roll-up criterion for synthetic jets, *AIAA Journal*, **47**, No. 5, 2009, 1252–1262.